Highly efficient and stable $Fe^{II}Fe^{III}$ LDH carbon felt cathode for removal of pharmaceutical ofloxacin at neutral pH

Weilu Yang[a,b,c,d], Minghua Zhou [b,c,*], Nihal Oturan[d], Mikhael Bechelany[e], Marc Cretin[e], Mehmet A. Oturan[d,*]

[a] *Guangdong Key Laboratory of Environmental Pollution and Health, School of Environment, Jinan University, Guangzhou 511443, China*

[b] *Key Laboratory of Pollution Process and Environmental Criteria, Ministry of Education, College of Environmental Science and Engineering, Nankai University, Tianjin 300350, China.*

[c] *Tianjin Key Laboratory of Environmental Technology for Complex Trans-Media Pollution, Nankai University, Tianjin 300350, P. R. China*

[d] *Université Paris-Est, Laboratoire Géomatériaux et Environnement, EA 4508, UPEM, 5 Bd Descartes, 77454 Marne-la-Vallée, Cedex 2, France.*

[e]*IEM (Institut Européen des Membranes), UMR 5635, CNRS, ENSCM, UM, Université de Montpellier, Place E. Bataillon, F-34095 Montpellier Cedex 5, France*

*: **Corresponding author's Email**

zhoumh@nankai.edu.cn (Minghua Zhou)

Mehmet.Oturan@univ-paris-est.fr (Mehmet A. Oturan)

Abstract

The traditional electro-Fenton (EF) has been facing major challenges including narrow suitable range of pH and non-reusability of catalyst. To overcome these drawbacks we synthesized $Fe^{II}Fe^{III}$-layered double hydroxide modified carbon felt ($Fe^{II}Fe^{III}$ LDH-CF) cathode via *in situ* solvo-thermal process. Scanning electron microscopy/Energy Dispersive X-Ray Spectroscopy (SEM/EDS) mapping and X-ray photoelectron spectroscopy (XPS) analysis of $Fe^{II}Fe^{III}$ LDH-CF illustrated the uneven distribution of Fe atom and existence of secondary phases such as $Fe(OH)_3$, Fe_2O_3, etc., on the modified cathode. Cyclic voltammetry and linear sweep voltammetry were operated to explore the electrochemical characterization of $Fe^{II}Fe^{III}$ LDH-CF cathode. The apparent rate constant of decay kinetics of ofloxacin (OFC) in heterogeneous EF with $Fe^{II}Fe^{III}$ LDH-CF (0.18 min^{-1}) was more than 3 times higher than that of homogeneous EF with 0.1 mM Fe^{2+} (0.05 min^{-1}) at current density of 9.37 mA cm^{-2}. A series of experiments including evolution of solution pH, iron leaching, OFC removal with trapping agent (tertiary butyl alcohol) and quantitative detection of •OH were conducted to explore the degradation mechanism in heterogeneous EF, demonstrating the dominant role of •OH generated by anodic oxidation (BDD(•OH)) and surface catalyst (•OH) via $\equiv Fe^{II}/Fe^{III}$ on LDH cathode for organics degradation, as well contributing to high efficiency and good stability at neutral pH. Besides, formation and evolution of aromatic intermediates, carboxylic acids and inorganic ions (F^-, NH_4^+ and NO_3^-) were identified and followed during OFC mineralization by high-performance liquid chromatography (HPLC), gas chromatography–mass spectrometry (GC-MS) and ionic chromatography analyses. These findings allowed proposing a plausible degradation pathway of OFC by hydroxyl radicals generated in

the process.

Keywords: Surface catalysis; Heterogeneous electro-Fenton; $Fe^{II}Fe^{III}$ LDH-CF; Ofloxacin; Reusability

1. Introduction

Presence of pharmaceuticals in the environment became a hot topic due to the serious problems caused to environmental safety and human health. Besides, these compounds have been detected in wastewater, ground waters and drinking waters at various concentrations in the range of μg L^{-1} to ng L^{-1} [1, 2]. Among pharmaceuticals, antibiotics are largely used since they play an important role in health care and cure systems for both human and animals. Ofloxacin (OFC), as one of the most common used antibiotic, especially for the cure of pneumonia, gonorrhea, skin infections, bronchitis and infections of the prostate, constitutes considerable threat to environment due to its extensive occurrence and genotoxic properties [3-5]. On the other hand, the conventional wastewater treatment methods are unfortunately inefficient in removing antibiotics, in general, and OFC specifically from water [6, 7].

As one of the most used eco-friendly electrochemical advanced oxidation processes, the electro-Fenton (EF) combining electrochemistry and classical Fenton reaction, has drawn much attention due to its environmental friendly character and great oxidation/mineralization efficiency against persistent organic pollutants. Indeed, this process generates hydroxyl radicals (•OH), a highly strong oxidant species, from the reaction between electrochemically produced H_2O_2 via oxygen reduction reaction

(eq. (1)) and externally added catalyst (Fe^{2+}) according to Fenton reaction (eq. (2)). Fe^{2+} consumed in Fenton reaction is then electrochemically regenerated from reduction of Fe^{3+} formed in eq. (2) [8-11]. Thereby, the recycle reaction (eq. (3)) between Fe^{3+} and Fe^{2+} guarantees the continuous generation of $^{\bullet}OH$.

$$O_2 + 2H^+ + 2e^- \rightarrow H_2O_2 \quad (1)$$

$$Fe^{2+} + H_2O_2 \rightarrow Fe^{3+} + OH^- + {}^{\bullet}OH \quad (2)$$

$$Fe^{3+} + e^- \rightarrow Fe^{2+} \quad (3)$$

In Fenton reaction and related processes, the optimum pH range is around 3 (2.8-3.0). Therefore, the solution pH has a great influence on the efficiency of EF process. At pH > 4, there is catalyst lost by precipitation under $Fe(OH)_3$, while at low pH, H_2O_2 is protonated to form hydroperoxonium ($H_3O_2^+$) ion (eq. (4)), which is less reactive with Fe^{2+} [10] and leads to a decrease in process efficiency.

$$H_2O_2 + H^+ \rightarrow H_3O_2^+ \quad (4)$$

Aiming to overcome these drawbacks, heterogeneous EF with natural iron containing minerals (goethite, magnetite, pyrite, chalcopyrite, etc.) as solid catalysis has been explored for the treatment of wastewater [12-16]. Various iron-containing or transition metal oxides as heterogeneous catalysts used alone or effectively combined with microporous and mesoporous support materials have also become research hotspots, with exhibiting remarkable catalytic activity and good reusability[17-19]. However, the use of this kind of solid catalysts involves their separation after treatment. On the other side, the complicated preparation routes and operation conditions for the synthetic electrode limit the development of practical applications

[20, 21]. Besides, leaching of metallic catalyst considered toxic such as Cu or Co has detrimental effect on environment during heterogeneous EF process[22]. In addition, it turns out that the super ability of contaminants adsorption would weaken the catalytic degradation in heterogeneous EF with micro/mesoporous material supporters [23]. Therefore, it is a challenge to develop kinds of cost efficient electrodes with nontoxic metals as catalyst meanwhile extending the applicable range of pH solution in heterogeneous EF process for wastewater treatment.

Recently, outstanding mineralization of organics have been reported as a result of both homogeneous EF and surface catalyzed heterogeneous EF [24]. In this study, heterogeneous $Fe^{II}Fe^{III}$-layered double hydroxide ($Fe^{II}Fe^{III}$ LDH) modified carbon felt (CF) cathode was prepared via solvothermal process with deposition of $Fe^{II}Fe^{III}$. The performance of heterogeneous EF with $Fe^{II}Fe^{III}$ LDH-CF cathode was overall evaluated and the mechanism of organics mineralization was deeply explored at neutral pH solution. Electrochemical characterizations such as cyclic voltammogram (CV), linear sweep voltammetry (LSV) and catalytic activity of $Fe^{II}Fe^{III}$ LDH-CF were evaluated and compared with unmodified carbon felt cathode. Boron-doped diamond (BDD) thin film electrode was chosen as anode because of its high oxidation/mineralization power in organic pollutants removal due to the generation of high amounts of heterogeneous hydroxyl radicals (BDD($^{\bullet}$OH)) (eq. (5)) during the process[25, 26].

$$BDD + H_2O \rightarrow BDD(^{\bullet}OH) + H^+ + e^- \quad (5)$$

Heterogeneous EF using BDD/$Fe^{II}Fe^{III}$ LDH-CF was successfully applied to the

mineralization of aqueous OFC solution, including mineralization efficiency and energy consumption studies and reusability test. Finally, formed oxidation intermediates and end-products were analyzed and a plausible mineralization pathway for OFC by hydroxyl radicals was proposed.

2. Materials and methods

2.1. Chemicals

CF was bought from Alfa Aesar. The chemicals for preparation of $Fe^{II}Fe^{III}$ LDH cathode including iron(II) sulfate heptahydrate ($FeSO_4 \cdot 7H_2O$) (> 99% purity), iron(III) nitrate nonahydrate, $Fe(NO_3)_3 \cdot 9H_2O$ (98% purity), urea $CO(NH_2)_2$ (≥ 99.0 % purity), ammonium fluoride (NH_4F) (99% purity) were provided by Sigma Aldrich. Analytical grade OFC ($C_{18}H_{20}FN_3O_4$, CAS nº: 82419-36-1, MW: 361.1 g mol^{-1}, 99.9% purity) was purchased from Alfa and was chosen as target pollutant without further purification. Acetonitrile and phosphoric acid were used as mobile phase of HPLC. Potassium titanium (IV) oxalate, dimethyl sulfoxide and 2,4-dinitrophenylhydrazine were used for measurement of $^{\bullet}OH$. Phenanthroline and hydroxylamine hydrochloride were used for detection of Fe^{2+} and total Fe in solution. Tertiary butyl alcohol (TBA) was chosen as trapping agent of $^{\bullet}OH$. Anhydrous sodium sulfate (Na_2SO_4, 99-100% purity) was used as supporting electrolyte in all of the experiments. Experimental solutions were prepared with deionized water and solution pH was adjusted with H_2SO_4 (1 M) and NaOH (1 M).

2.2. Preparation and characterization of $Fe^{II}Fe^{III}$ LDH–CF electrode

The $Fe^{II}Fe^{III}$ LDH modified CF cathode was synthesized via *in situ* solvo-thermal process using Teflon lining autoclave containing mixture solution of $FeSO_4 \cdot 7H_2O$ (25 mM), $Fe(NO_3)_3 \cdot 9H_2O$ (12.5 mM), NH_4F (125 mM) and $Co(NH_2)_2$ (0.5 M) and 90 mL deionized water [27, 28]. The CF (4×8 cm^2) was pretreated with concentrated HNO_3, and subsequently cleaned via ultrasonication with acetone, ethanol and deionized water successively and then transferred into the Teflon-lined autoclave for hydrothermal treatment at about 100 ºC. The mass-loading of $Fe^{II}Fe^{III}$ was measured from the weight difference before and after the growth and calculated to be 0.15 g.

LSV was used to compare the electrochemical behavior of raw CF and $Fe^{II}Fe^{III}$ LDH-CF cathodes with the CHI660D workstation (from Shanghai Chenhua Corporation) at a scan rate of 50 mV s^{-1} in a three-electrode cell system. The raw CF or $Fe^{II}Fe^{III}$ LDH-CF cathode was used as the working electrode, respectively, a platinum sheet was chosen as the counter electrode and a saturated calomel electrode as the reference electrode. The measures were operated at ambient temperature.

Electroactive surface area is often recognized to be related to the surface chemistry of carbon-based electrodes [29-31]. In order to measure the electroactive surface areas of $Fe^{II}Fe^{III}$ LDH-CF and unmodified CF cathodes, CV experiments were carried out in saturated O_2 solution and the calculation was done according to Randles-Sevcik equation (eq. (6)) [32, 33]

$$I_p = 2.69\times10^5 \times A\, D^{\frac{1}{2}}\, n^{\frac{1}{2}}\, \upsilon^{\frac{1}{2}}\, C \qquad (6)$$

Where I_P is the peak current (A), n is the number of electrons involving in the redox reaction (n=1), A is the area of the electrode (cm^2), D is the diffusion coefficient of the molecule in solution (7.6×10^{-6} cm^2 s^{-1}), C is the concentration of the probe molecule in the bulk solution (1×10^{-5} cm^3) and *v* is the scan rate (0.01 V s^{-1}).

The structure of the synthesized $Fe^{II}Fe^{III}$ LDH-CF cathode was analyzed by X-ray photoelectron spectroscopy (XPS) (Krato-ultra DLD, Shimazduo). Surface morphology of $Fe^{II}Fe^{III}$ LDH-CF cathode was analyzed by scanning electron microscopy (SEM, SHIMADZU SS-550) and energy dispersive X-ray spectroscopy (EDS) using instrument GENESIS (from EDAX, China) respectively.

2.3. Electrochemical cell

The experiments were carried out in a 250 mL open reactor containing 0.1 mM OFC and stirred by magnetic bar in the bottom, meanwhile with aeration at flow rate of 0.75 L min^{-1} to make sure the saturated oxygen condition. All the electrodes had a surface area of 4×8 cm^2. BDD electrode was used as anode and the prepared $Fe^{II}Fe^{III}$ LDH-CF or unmodified CF were used as cathode. 230 mL OFC (0.1 mM) solution containing 50 mM Na_2SO_4 as electrolyte was adjusted to pH 7. All of the experiments were carried out triplicate and operated at ambient temperature.

2.4. Instruments and analytical procedures

The concentration decay of OFC was monitored by HPLC (U3000, Thermo Scientific, USA) on a C18 column (3 μm, 3.0 mm (i.d.), 100 mm) with diode array detector (wavelength at 288 nm). The analytical conditions were as follows: the

mobile phase was 15% acetonitrile, 1% phosphoric acid and 84% water with a flow rate of 0.3 mL min^{-1}. The evolution of TOC of 0.1 mM OFC solution (21.6 mg L^{-1} TOC theoretically) during treatment was measured by TOC analyzer (Analytikjena multi N/C 3100, Germany) to assess the mineralization rate of OFC in heterogeneous EF process, and the mineralization current efficiency (MCE) of OFC solution during the electrochemical degradation process was calculated according to following equation [34, 35]:

$$MCE(\%) = \frac{n\,F\,V_s\,\Delta(TOC)_{exp}}{4.32 \times 10^7 m\,I\,t} \times 100 \qquad (7)$$

Where *n* is the number of electrons consumed per OFC molecule and was taken as 74 according to mineralization reaction presented in eq. (8) assuming that the majority of N contains in OFC molecule was released as NH_4^+ [36], F represents the Faraday constant (96485 C mol^{-1}), $\Delta(TOC)_{exp}$ means the TOC decay at t time, V_s is the volume of electrolyte solution (L), 4.32×10^7 represents a conversion factor to homogenize units (3600 s h^{-1} × 12000 mg of C mol^{-1}), *I* is the current applied (A), t is the electrolysis time (h) and m is the number of carbon atoms (18) of OFC.

$$C_{18}H_{20}FN_3O_4 + 32H_2O \rightarrow 18CO_2 + F^- + 3NH_4^+ + 72H^+ + 74\,e^- \qquad (8)$$

Besides, energy consumption (EC) is another parameter should be taken into consideration to evaluate the performance of cathode relating the cost effectiveness of organics degradation process, which was measured in the unit of kWh energy per g TOC removal and calculated as following [37]:

$$EC = \frac{U\ I\ t}{(\Delta TOC)_t\ V_s} \quad (9)$$

where U, I, t are the average cell voltage (V), the current applied (A) and the electrolysis time (h), respectively and V_s is the solution volume (L).

Additionally, the concentration of ·OH generated during the electrochemical process was measured from its reacted with dimethyl sulfoxide trapping and 2,4-dinitrophenylhydrazine reagent forming a kind of corresponding hydrazone (HCHO-DNPH), and was quantitatively detected by HPLC described above with a diode array detector set at 355 nm [38, 39].

Besides, the organic intermediate products of OFC degradation in heterogeneous EF were identified and detected by GC-MS (Agilent, 7890 A/5975 C, USA) with a HP-5MS column (30 m, 0.25 mm × 0.25 μm) and an electrospray ionization source with helium gas as the carrier gas at flow rate of 1.0 mL min^{-1}. The operation condition of GC-MS was set as: initial column temperature was 55 ^{o}C for 3 min, and increased to 300 ^{o}C with 10 ^{o}C min^{-1} and held for 5 min at this temperature.

Short-chain carboxylic acids formed during the mineralization process were identified and detected by HPLC (Agilent, 1260, USA) with a Carbomix H-NP10 column (6.0 μm, 7.8×300 mm) at wavelength of 210 nm. H_2SO_4 (0.25 mM) was chosen as mobile phase at flow rate of 0.6 mL min^{-1}.

The concentration of H_2O_2 was detected via the potassium titanium (IV) oxalate method at wavelength of 400 nm with UV-Vis spectrophotometer (UV795 Shanghai

Instrument Analysis Co. Ltd). Concentration of Fe^{2+} leached to the solution was determined by spectrophotometric method at 510 nm via its complex with phenanhroline and with addition of hydroxylamine hydrochloride for total iron detection.

3. Results and discussion

3.1. Characterization of synthesized $Fe^{II}Fe^{III}$ LDH-CF cathode

The morphology of prepared $Fe^{II}Fe^{III}$ LDH-CF cathode was observed by SEM and the results were shown in Fig. 1. It can be seen that each strand of the CF was covered with amounts of formed dense particles of $Fe^{II}Fe^{III}$ LDH, which can be observed clearly via the magnified image of Fig. 1(b) and Fig. 1(c). Besides, a small part of $Fe^{II}Fe^{III}$ LDH-CF (inset of Fig. 1(b)) was taken out and analyzed by EDS mapping test and the scanning result of Fig. 1(f) shows the inhomogeneous distribution of Fe atoms on the surface of CF.

The SEM/EDS results of $Fe^{II}Fe^{III}$ LDH-CF were presented in Figs. 2(a) and 2(b). Two sample spots were taken without particles covering. The data analyzed of dots 1 and 2 show that there are only carbon and oxygen elements exist in these two sites. Fig. 2(b) depicted the scanned results of samples with deposited particles on $Fe^{II}Fe^{III}$ LDH-CF. The contents of Fe exist in space 1 and 2 were shown as 5.4% and 3.9%, which also illustrates the uneven distribution of Fe atom on $Fe^{II}Fe^{III}$ LDH-CF.

The crystalline phase of modified $Fe^{II}Fe^{III}$ LDH-CF was detected by XRD, and the diffraction patterns are shown in Fig. 2(c). Layered structure of hydrotalcite-like

phase was represented by diffraction peaks at 2θ values of 6°, 12°, 18° and 22°. Distinct peaks between 30° and 55° 2θ indicating the extensive crystal growth. The diffraction peaks at 22°, 32° and 35° 2θ corresponding to the existence of secondary phases in the modified CF cathode including $Fe(OH)_3$, Fe_2O_3 and maghemite Fe_2O_3, and 62° 2θ indicates the transformation between $Fe(OH)_3$ and Fe_2O_3 [24, 40]. Besides, the diffraction peaks around 24° and 43° 2θ are ascribed to the carbon content of $Fe^{II}Fe^{III}$ LDH-CF [24].

XPS presented the chemical composition of raw CF and $Fe^{II}Fe^{III}$ LDH-CF (Fig. 2(d)) and contents of atoms were showed in Table 1. The atomic carbon content of CF significantly decreased after modification with $Fe^{II}Fe^{III}$ LDH, which was only half of the raw one. Obviously, the content of Fe2p increased from 0.9% to 34.4%, illustrating the successful modification compared to raw CF, as well as the detected elements such as Fe (2p3, 2p1) and increasing nitrogen content. Especially, the peaks of Fe 2p3, Fe 2p1 around 720 eV and 732 eV, respectively, can be split into Fe 2p3/2 (711 eV) and Fe 2p1/2 (725 eV).

3.2. Electrochemical characterization of synthesized $Fe^{II}Fe^{III}$ LDH-CF cathode

LSV of $Fe^{II}Fe^{III}$ LDH-CF and raw CF electrodes were depicted in Fig. 3(a). The current density of $Fe^{II}Fe^{III}$ LDH-CF (7.9 mA cm^{-2}) was two times higher of the raw CF (3.9 mA cm^{-2}) in O_2 saturated solution at a scan rate of 50 mV s^{-1} with providing more potential of accelerating electrons transfer rate during electrochemical oxidation process. Also, the CV curves of raw CF and $Fe^{II}Fe^{III}$ LDH-CF cathodes were carried

out in 10 mM $[Fe(CN)_6]^{3-}/[Fe(CN)_6]^{4-}$ solution (Fig. 3(b)), and a 2.5-fold increase of the peak current was observed on $Fe^{II}Fe^{III}$ LDH-CF, proving much more active sites compared to unmodified one. The electroactive surface areas were calculated to be 42 cm^2 (raw CF) and 127 cm^2 ($Fe^{II}Fe^{III}$ LDH-CF) according to eq. (6). The 3 times improvement of electroactive surface area would contribute to a higher rate of electrochemical reactions on the cathode.

In order to further explore the electrocatalytic activity of modified cathode, a series of comparative experiments were operated for the decay kinetics of target pollutants OFC (0.1 mM) with raw CF and $Fe^{II}Fe^{III}$ LDH-CF under different current densities ranging from 3.12 to 12.5 mA cm^{-2} (Figs. 3(c) and 3(d)). It should be pointed out here, in the homogeneous EF process with raw CF, the concentration of Fe^{2+} was 0.1 mM，which was optimized as the most proper concentration of Fe^{2+} in previous study [9], in contrast, no additional iron ion was added in the heterogeneous EF with $Fe^{II}Fe^{III}$ LDH-CF. In both cases the removal efficiency and decay kinetics of OFC increased with the increasing current density. The results in Fig. 3(c) show that the complete disappearance of OFC obtained at 50 min and 60 min with 12.5 mA cm^{-2} and 9.37 mA cm^{-2} in EF with raw CF cathode, while in the heterogeneous EF with $Fe^{II}Fe^{III}$ LDH-CF, OFC was completely disappeared at 30 min under same conditions of current density (9.37 and 12.5 mA cm^{-2}). What is more, the total disappearance of OFC was achieved at 40 min with 6.25 mA cm^{-2} with $Fe^{II}Fe^{III}$ LDH-CF cathode (Fig. 3(d)) while it needed 50 min with a current 2-times larger with raw CF cathode (Fig. 3(c)). The comparative results of apparent rate constant (k_{app}) values of decay kinetics

of OFC in different systems were presented in Table 2. As can be seen from this Table, the k_{app} values in heterogeneous EF with $Fe^{II}Fe^{III}$ LDH-CF cathode were approximately 3 times of the results in homogeneous EF with raw CF at current density of 3.12, 6.25 and 9.37 mA cm^{-2}, which was in agreement with the performances showed in Figs. 3(c) and 3(d), demonstrating again the high efficiency of $Fe^{II}Fe^{III}$ LDH-CF cathode for OFC degradation.

3.3. Mineralization performance of $Fe^{II}Fe^{III}$ LDH-CF in heterogeneous EF

As it is evident, the formation of certain intermediate products would lead to various environmental pollutions during the treatment of organics by advanced oxidation processes [41, 42]. In this context and aiming to explore the performance of heterogeneous EF with $Fe^{II}Fe^{III}$ LDH-CF for in complete mineralization of OFC solution, TOC removal experiments were conducted for 8 h and results are depicted in Fig. 4. Fig. 4(a) shows that OFC and its intermediate products could be completely removed at 8 h electrolysis with current densities of 12.5 mA and 9.37 mA cm^{-2}, while TOC removal efficiency was 88% and 71% at 8 h with current densities of 6.25 and 3.12 mA cm^{-2}, respectively. The inset depicts the evolution of MCE% during the mineralization process of OFC solution, which attained their peak values at early stage of the mineralization experiment with different current densities. Afterwards, the MCE% values kept diminishing with increasing current densities until the end of treatment time (8 h). This can be explained by the generation of less easily oxidized short-chain carboxylic acids as well as the reduction of concentration of OFC in the solution slowing down mass transport rate to BDD anode [9, 43, 44]. Also, it can be

observed that the trend of MCE% with increasing current density was opposite to the evolution of TOC with obtaining the highest values at 3.12 mA cm^{-2} because of enhancement of the wasting reactions such as H_2 evolution at cathode and O_2 generation at anode with high current densities, which also rose the EC during the mineralization process (Fig. 4(b)). The EC increased as current density increasing from 3.12 to 12.5 mA cm^{-2}, reaching to 0.74, 1.38, 2.05 and 3.16 kWh $(g\ TOC)^{-1}$ at treatment time of 8 h with current density of 3.12, 6.25, 9.37 and 12.5 mA cm^{-2}, respectively.

Additionally, the comparative experiments of TOC degradation, MCE% and EC values evolution in homogeneous EF with raw CF at current density of 9.37 and 12.5 mA cm^{-2} were studied and presented in Figs. 4(c) and 4(d). It is evident that the performance of TOC removal efficiencies in heterogeneous EF with $Fe^{II}Fe^{III}$ LDH-CF were much outstanding compared to homogeneous EF with raw CF. The comparative plots of MCE% and EC evolution as the function of electrolysis time also proved the cost-efficient characteristic of $Fe^{II}Fe^{III}$ LDH-CF for wastewater treatment.

3.4. Mechanism of OFC mineralization with $Fe^{II}Fe^{III}$ LDH-CF

During mineralization process of OFC solution in heterogeneous EF with $Fe^{II}Fe^{III}$ LDH-CF cathode, the degradation efficiency can be regarded as a combined contribution of three parts: i) the anodic oxidation via BDD(•OH) generated at the surface of BDD anode (eq. (5)), ii) oxidation by homogeneous •OH generated via the reaction of H_2O_2 with Fe^{2+} leached from $Fe^{II}Fe^{III}$ LDH-CF (eq. (2)), and heterogeneous catalysis process via Fe^{II}/Fe^{III} on surface of $Fe^{II}Fe^{III}$ LDH-CF cathode.

Therefore, pH plays an important role in degradation and mineralization of organic pollutants, especially in the heterogeneous EF with solid catalysts [45].

The results of pH evolution and concentration of Fe^{2+} and total Fe leached in solution were detected (with initial solution pH adjusted to 7). The results in Fig. 5(a) depict that a sharp decreasing of pH occurred at the early stage of OFC mineralization in heterogeneous EF with $Fe^{II}Fe^{III}$ LDH-CF, which can be attributed to the gradual formation of carboxylic acids during the mineralization of OFC [10, 25], and then pH slowly increased from 4.5 to 4.7. After 4 h treatment of OFC solution, the pH value kept constant (pH 4.7) until the end of electrolysis time of 8 h. Meanwhile, the concentration of Fe^{2+} and total Fe leached from $Fe^{II}Fe^{III}$ LDH-CF during mineralization of OFC were reported in Fig. 5(b). The results depict that 0.2 mg L^{-1} Fe^{2+} and 0.32 mg L^{-1} total Fe were detected at treatment time of 8 h, demonstrating the non-significant contribution of the effect of Fe^{2+}/Fe^{3+} catalytic cycle for generation of homogeneous $^{\bullet}OH$ in solution.

Further, the yield of H_2O_2 generation and quantities of $^{\bullet}OH$ in heterogeneous EF with $Fe^{II}Fe^{III}$ LDH-CF and homogeneous EF with raw CF (with addition of 0.1 mM Fe^{2+}) were identified at different time at pH 7. The comparative results in Fig. 5(c) demonstrate that the amounts of $^{\bullet}OH$ generation in heterogeneous EF with $Fe^{II}Fe^{III}$ LDH-CF cathode was much higher than that in homogeneous EF with 0.1mM Fe^{2+}. This unexpected high concentration of $^{\bullet}OH$ in heterogeneous EF seems inconsistent to the amounts of Fe^{2+} leaching in solution and the low concentration of H_2O_2 generation on the cathode. The main reason is because of the loss of catalyst by precipitation in

homogeneous EF at pH 7, the other can be attributed to the high catalytic activity of $Fe^{II}Fe^{III}$ LDH on modified CF cathode with activating H_2O_2 to $^{\bullet}OH$ for organics degradation.

Inevitably, the anodic oxidation would make contribution to OFC degradation [10, 46] with heterogeneous BDD($^{\bullet}OH$) formed at the surface of BDD anode [41]. Comparatively, $Fe^{II}Fe^{III}$ LDH-CF was replaced by stainless steel, thus eliminating the contribution of homogeneous $^{\bullet}OH$ in solution. The results in Fig. 5(d) present that degradation efficiency of 52% was attained in AO with stainless steel cathode, illustrating that more than 40% contribution to OFC oxidation was made by metal oxides catalyzed process in heterogeneous EF with $Fe^{II}Fe^{III}$ LDH-CF cathode. Besides, TBA was added into solution as trapping agent of $^{\bullet}OH$ in heterogeneous EF with $Fe^{II}Fe^{III}$ LDH-CF cathode at pH 7. The removal efficiency significantly decreased from 100% to 34% at 20 min, demonstrating the dominant role of $^{\bullet}OH$ for OFC removal.

According to the analysis above, a mechanism for OFC destruction in heterogeneous EF with $Fe^{II}Fe^{III}$ LDH-CF was proposed. The significant removal efficiency of heterogeneous EF with $Fe^{II}Fe^{III}$ LDH-CF at pH 7 was mainly due to the surface catalyzed process occurring at the solid-liquid interface, avoiding the formation of iron hydroxide precipitation at this pH in contrast to homogeneous EF. The contribution of $^{\bullet}OH$ to OFC mineralization is mainly from two sources: heterogeneous BDD($^{\bullet}OH$) via anodic oxidation and surface iron oxides catalysis by $\equiv Fe^{II}/Fe^{III}$ cycle. The in-situ generated H_2O_2 on $Fe^{II}Fe^{III}$ LDH-CF could be

decomposed to •OH via heterogeneous Fenton reaction according to eq. (10). ≡ Fe^{III}—OH formed at the cathode surface is then electrochemically reduced to ≡ Fe^{II}—OH ((eq. 11)). Fe^{III}—OH also could directly react with H_2O_2 to form a kind of surface complex product of H_2O_2 (≡ Fe^{III}—$OH(H_2O_2)$s), which may undergo a reversible ground-state electron transfer and to be further activated to ≡Fe^{II}—OH (eq. (12)-(14)). Therefore, in neutral pH solution, the rate of reaction (14) would be accelerated to catalyze the formation of homogeneous •OH via eq. (10) [24, 45] with formation of an additional oxidant $HO_2^{\bullet}$ (E° = 1.70 V/SHE); thus providing more potential process for the treatment of industrial wastewater at neutral or alkaline pH.

$$\equiv Fe^{II}\text{—}OH + H_2O_2 \rightarrow \equiv Fe^{III}\text{—}OH + {}^{\bullet}OH + OH^- \quad (10)$$

$$\equiv Fe^{III}\text{—}OH + e^- \rightarrow \equiv Fe^{II}\text{—}OH \quad (11)$$

$$\equiv Fe^{III}\text{—}OH + H_2O_2 \rightarrow \equiv Fe^{III}\text{—}OH(H_2O_2)(s) \quad (12)$$

$$\equiv Fe^{III}\text{—}OH(H_2O_2)(s) \rightarrow \equiv Fe^{II}\text{—}OH(HO_2^{\bullet})(s) + H^+ \quad (13)$$

$$\equiv Fe^{II}\text{—}OH(HO_2^{\bullet})(s) \rightarrow \equiv Fe^{II}\text{—}OH + HO_2^{\bullet} \quad (14)$$

3.5. Reusability of $Fe^{II}Fe^{III}$ LDH-CF cathode for OFC removal

Generally, the stability and reusability of $Fe^{II}Fe^{III}$ LDH-CF significantly related to the pH of solution. At neutral or alkaline condition, the stability of LDH is hardly affected [47]. The results of decay kinetics of OFC and TOC decay for 6 cycles were presented in Fig. 6. It is necessary to note that after each experiment the cathode was mildly washed and the treated OFC solution was replaced by fresh one. In terms of

decay kinetics, the complete degradation of 0.1 mM OFC was always attained in 1 h over 6 cycles (Fig. 6(a)), exhibiting excellent stability of the catalytic activity of $Fe^{II}Fe^{III}$ LDH-CF cathode for reusability. Similarly, 96% and 95% removal efficiency of TOC were obtained for the first two cycles after 6 h, and about 84% of TOC degradation efficiency was observed after 6 cycles. The 12% reduction in TOC removal efficiency confirms a slight loss of the catalytic activity of $Fe^{II}Fe^{III}$ LDH-CF cathode for recycle, which can be attributed to the outstanding stability of LDH particles on modified cathode at neutral pH solution.

3.6. Evolution of carboxylic acids and inorganic ions

The oxidative degradation of OFC and its intermediates along with oxidative cleavage of aromatic organics leads to the formation of a variety of short-chain carboxylic acids, which have been reported to be resistant to the attack by $^{\bullet}OH$ and usually need very long time for complete mineralization [37, 48]. The identification of carboxylic acids generated during mineralization of OFC solution and their evolution in heterogeneous EF with $Fe^{II}Fe^{III}$ LDH-CF cathode at pH 7 are depicted Fig. 7(a). Acetic, maleic, formic, fumaric, oxamic and oxalic acids detected at retention time of 9.3, 10.4, 13.2, 14.5, 15.6 and 15.8 min, respectively. Maleic and formic acids were detected at trace level (< 0.05 mM) during the process and were not presented in Fig. 7(a). All of the carboxylic acids were accumulated quickly at the first stage of treatment time, and subsequently their concentration decreased with the increasing electrolysis time. With BDD anode, the peak value of oxalic acid concentration (0.27

mM) was obtained at approximately 120 min. It is generally regarded as the final organic acids before the end of complete mineralization of pollutants and intermediate products [9, 49]. Maximum concentrations of acetic (0.11 mM) and oxamic (0.09 mM) acids were attained at 60 min. These results are consistent with the results of TOC removal Fig. 4(a).

Generally, the identification and evolution of inorganic ions (corresponding to heteroatoms present in mother pollutant) constitute an important reference signal for mineralization of organic pollutants. OFC contains F and N atoms that can be oxidized to inorganic ions F^-, NH_4^+, NO_2^- and NO_3^-. The evolution of F^-, NH_4^+ and NO_3^- was presented in Fig. 7(b), while NO_2^- was not detected in this study. As can be seen, the concentration of F^- generated increased rapidly and reached the maximum value at the first 2 h, afterwards kept constant along with treatment time until 8 h. The quasi-constant quantity of F^- (0.1 mM) was in accordance with the theoretical value of F atom in OFC molecule. The amounts of NH_4^+ detected continuously increased with treatment time and attained 0.21 mM at the end of 8 h, whereas the result was different in the case of NO_3^-. The concentration of NO_3^- firstly increased with electrolysis time reaching the maximum value of 0.09 mM at 4 h, and then slowly diminished until the end of treatment, which was consistent to the results already reported [50]. Since the oxamic acid was not detected at 8 h (it is completely removed at 4 h), the sum of NH_4^+ and NO_3^- was calculated as 0.26 mM, reaching 86.7% of the total nitrogen contents of 0.3 mM, the maximum concentration of N in initial solution. The slight difference can be attributed to the generation of undetected gases (N_2, N_2O_5,

NO_x) at the cathode via reduction of NO_3^- [50, 51].

3.7. Reaction pathway for the mineralization of OFC during EF with $Fe^{II}Fe^{III}$ LDH-CF cathode

Based on the OFC transformation products (OTPs) detected by HPLC and GC-MS (Table 3), a plausible degradation pathway of OFC in heterogeneous EF has been proposed as shown in Fig. 8. The carboxyl group of OFC molecule was attacked by •OH with generation of OTP 1 (which was not detected in this study, probably because of its quick transformation; but has been reported in previous study [52, 53]) via decarboxylation reaction, which was in agreement with the results already reported. Indeed carboxyl group is prone to the reaction with •OH because of its negative charge (since •OH is an electrophilic species) [54]. OTP 2 was formed from cleavage of piperazinyl group via further attack of •OH. Meanwhile, OTP 3 was produced via defluorination, which was then further attacked by •OH via breaking of piperazinyl ring and causing dealkylation, with the formation of OTP 4. The subsequent progressive oxidative degradation undergoes oxidative cleavage of aromatic ring, leading to the formation of carboxylic acids (OTP 5-9) before completely mineralized to CO_2, H_2O and inorganic ions (NH_4^+ and NO_3^-).

4. Conclusions

In this study, synthesized $Fe^{II}Fe^{III}$ LDH-CF cathode was prepared and its performance was tested in EF process at neutral pH without adding Fe^{2+} (catalyst of

conventional EF) for OFC degradation as target pollutant. It was proved that the heterogeneous EF with modified cathode could improve the removal efficiency of organic pollutant compared to homogeneous EF at pH 7. Complete TOC removal was attained at 8 h electrolysis with applied current density of 9.37 mA cm^{-2}. A series of designed experiments proved that surface iron oxides catalysis via $\equiv Fe^{II}/Fe^{III}$ contributes to the significant performance of heterogeneous EF for organics removal at pH 7 with great stability. Formation and evolution of short-chain carboxylic acids and complete release of inorganic ions during mineralization process confirmed the outstanding behavior of $Fe^{II}Fe^{III}$ LDH-CF cathode for effective treatment of water containing OFC as organic pollutant at neutral pH conditions.

Acknowledgement

This work was financially supported by National Natural Science Foundation of China (nos. 21773129, 21811530274, 21976096 and 21273120), National Key Research and Development Program of China (2016YFC0400706), Tianjin Science and Technology Program (19PTZWHZ00050), Tianjin Development Program for Innovation and Entrepreneurship, National High-level Foreign Experts Project (G20190002011), 111 program, Ministry of Education of the People's Republic of China (T2017002) and Fundamental Research Funds for the Central Universities, Nankai University.

References

[1] E. Hapeshi, A. Achilleos, M.I. Vasquez, C. Michael, N.P. Xekoukoulotakis, D. Mantzavinos, D. Kassinos, Drugs degrading photocatalytically: kinetics and mechanisms of ofloxacin and atenolol removal on titania suspensions, Water Res. 44 (2010) 1737-1746.

[2] E. Hapeshi, I. Fotiou, D. Fatta-Kassinos, Sonophotocatalytic treatment of ofloxacin in secondary treated effluent and elucidation of its transformation products, Chem. Eng. J. 224 (2013) 96-105.

[3] K.W. Goyne, J. Chorover, J.D. Kubicki, A.R. Zimmerman, S.L. Brantley, Sorption of the antibiotic ofloxacin to mesoporous and nonporous alumina and silica, J. Colloid. Interf. sci 283 (2005) 160-170.

[4] C.C. Jara, D. Fino, V. Specchia, G. Saracco, P. Spinelli, Electrochemical removal of antibiotics from wastewaters, Appl. Catal. B: Environ. 70 (2007) 479-487.

[5] K. Kümmerer, A.A. Ahmad, V.M. Sundermann, Biodegradability of some antibiotics, elimination of the genotoxicity and affection of wastewater bacteria in a simple test, Chemosphere 40 (2000) 701-710.

[6] I. Michael, E. Hapeshi, C. Michael, D.F. Kassinos, Solar Fenton and solar TiO_2 catalytic treatment of ofloxacin in secondary treated effluents: evaluation of operational and kinetic parameters, Water Res. 44 (2010) 5450-5462.

[7] R.O. Pérez, J.R. Utrilla, M.S. Polo, J.L. Peñalver, R.L. Ramos, Degradation of antineoplastic cytarabine in aqueous solution by gamma radiation, Chem. Eng. J. 174 (2011) 1-8.

[8] G.B. Ren, M.H. Zhou, P. Su, W.L. Yang, X.Y. Lu, Y.Q. Zhang, Simultaneous sulfadiazines degradation and disinfection from municipal secondary effluent by a flow-through electro-Fenton process with graphene-modified cathode, J. Hazard. Mater. 368 (2019) 830-839.

[9] W.L. Yang, M.H. Zhou, N. Oturan, Y. Li, M.A. Oturan, Electrocatalytic destruction of pharmaceutical imatinib by electro-Fenton process with graphene-based cathode, Electrochim. Acta 305 (2019) 285-294.

[10] M.A. Oturan, J.J. Aaron, Advanced oxidation processes in water/wastewater treatment: principles and applications. A review, Crit. Rev. Env. Sci. Technol. 44 (2014) 2577-2641.

[11] M.H. Zhou, M.A. Oturan, I. Sirés, Electro-Fenton Process: New Trends and Scale-Up (ISBN: 978-981-10-6405-0) in: The Handbook of Environmental

Chemistry, volume 61, 2017, Springer, Singapour, 2017.

[12] C.M.S. Sánchez, E. Exposito, J. Casado, V. Montiel, Goethite as a more effective iron dosage source for mineralization of organic pollutants by electro-Fenton process, Electrochem. Commun. 9 (2007) 19-24.

[13] E. Expósito, C.M. Sánchez-Sánchez, V. Montiel, Mineral iron oxides as iron source in electro-Fenton and photoelectro-Fenton mineralization processes, J. Electrochem. Soc. 154 (2007) 116-122.

[14] L. Labiadh, M.A. Oturan, M. Panizza, N.B. Hamadi, S. Ammar, Complete removal of AHPS synthetic dye from water using new electro-fenton oxidation catalyzed by natural pyrite as heterogeneous catalyst, J. Hazard. Mater. 297 (2015) 34-41.

[15] N. Barhoumi, N. Oturan, H.O. Vargas, E. Brillas, A. Gadri, S. Ammar, M.A. Oturan, Pyrite as a sustainable catalyst in electro-Fenton process for improving oxidation of sulfamethazine. Kinetics, mechanism and toxicity assessment, Water Res. 94 (2016) 52-61.

[16] N. Barhoumi, L. Labiadh, M.A. Oturan, N. Oturan, A. Gadri, S. Ammar, E. Brillas, Electrochemical mineralization of the antibiotic levofloxacin by electro-Fenton-pyrite process, Chemosphere 141 (2015) 250-257.

[17] B. Hou, H. Han, S. Jia, H. Zhuang, P. Xu, D. Wang, Heterogeneous electro-Fenton oxidation of catechol catalyzed by nano-Fe_3O_4: kinetics with the Fermi's equation, J. Taiwan Inst. Chem. E. 56 (2015) 138-147.

[18] G. Zhang, Y. Zhou, F. Yang, FeOOH-catalyzed heterogeneous electro-Fenton system upon anthraquinone@ graphene nanohybrid cathode in a divided electrolytic cell: catholyte-regulated catalytic oxidation performance and mechanism, J. Electrochem. Soc. 162 (2015) H357-H365.

[19] S.B. Hammouda, F. Fourcade, A. Assadi, I. Soutrel, A. Amrane, L. Monser, Effective heterogeneous electro-Fenton process for the degradation of a malodorous compound, indole, using iron loaded alginate beads as a reusable catalyst, Appl. Catal. B: Environ. 182 (2016) 47-58.

[20] H. Zhao, Y. Chen, Q. Peng, Q. Wang, G. Zhao, Catalytic activity of MOF (2Fe/Co)/carbon aerogel for improving H_2O_2 and OH generation in solar photo–electro–Fenton process, Appl. Catal. B: Environ. 203 (2017) 127-137.

[21] H. Zhao, L. Qian, X. Guan, D. Wu, G. Zhao, Continuous bulk FeCuC aerogel with ultradispersed metal nanoparticles: an efficient 3D heterogeneous

electro-Fenton cathode over a wide range of pH 3–9, Environ. Sci. Technol. 50 (2016) 5225-5233.

[22] S.O. Ganiyu, T.X.H. Le, M. Bechelany, G. Esposito, E.D. Van Hullebusch, M.A. Oturan, M. Cretin, A hierarchical CoFe-layered double hydroxide modified carbon-felt cathode for heterogeneous electro-Fenton process, J. Mater. Chem. A 5 (2017) 3655-3666.

[23] E.G. Ramírez, M. Mora, J. Marco, M.U. Zañartu, Characterization of nanostructured allophane clays and their use as support of iron species in a heterogeneous electro-Fenton system, Appl. Clay. Sci. 86 (2013) 153-161.

[24] S.O. Ganiyu, T.X.H. Le, M. Bechelany, N. Oturan, S. Papirio, G. Esposito, E. Van Hullebusch, M. Cretin, M.A. Oturan, Electrochemical mineralization of sulfamethoxazole over wide pH range using FeIIFeIII LDH modified carbon felt cathode: degradation pathway, toxicity and reusability of the modified cathode, Chem. Eng. J. 350 (2018) 844-855.

[25] F. Sopaj, N. Oturan, J. Pinson, F. Podvorica, M.A. Oturan, Effect of the anode materials on the efficiency of the electro-Fenton process for the mineralization of the antibiotic sulfamethazine, Appl. Catal. B: Environ. 199 (2016) 331-341.

[26] M. Panizza, G. Cerisola, Direct and mediated anodic oxidation of organic pollutants, Chem. Rev. 109 (2009) 6541-6569.

[27] J. Zhao, J. Chen, S. Xu, M. Shao, D. Yan, M. Wei, D.G. Evans, X. Duan, CoMn-layered double hydroxide nanowalls supported on carbon fibers for high-performance flexible energy storage devices, J. Mater. Chem. A (2013) 8836-8843.

[28] X. Cai, X. Shen, L. Ma, Z. Ji, C. Xu, A. Yuan, Solvothermal synthesis of NiCo-layered double hydroxide nanosheets decorated on RGO sheets for high performance supercapacitor, Chem. Eng. J. 268 (2015) 251-259.

[29] W. Chen, X. Yang, J. Huang, Y. Zhu, Y. Zhou, Y. Yao, C. Li, Iron oxide containing graphene/carbon nanotube based carbon aerogel as an efficient E-Fenton cathode for the degradation of methyl blue, Electrochim. Acta 200 (2016) 75-83.

[30] Y.S. Grewal, M.J. Shiddiky, S.A. Gray, K.M. Weigel, G.A. Cangelosi, M. Trau, Label-free electrochemical detection of an Entamoeba histolytica antigen using cell-free yeast-scFv probes, Chem. Commun. 49 (2013) 1551-1553.

[31] W.L. Yang, M.H. Zhou, L. Liang, Highly efficient in-situ metal-free electrochemical advanced oxidation process using graphite felt modified with

N-doped graphene, Chem. Eng. J. 338 (2018) 700-708.

[32] T.X.H. Le, M. Bechelany, S. Lacour, N. Oturan, M.A. Oturan, M. Cretin, High removal efficiency of dye pollutants by electron-Fenton process using a graphene based cathode, Carbon 94 (2015) 1003-1011.

[33] W.L. Yang, M.H. Zhou, J.J. Cai, L. Liang, G.B. Ren, L.L. Jiang, Ultrahigh yield of hydrogen peroxide on graphite felt cathode modified with electrochemically exfoliated graphene, J. Mater. Chem. A 5 (2017) 8070-8080.

[34] M. Panizza, A. Dirany, I. Sirés, M. Haidar, N. Oturan, M.A. Oturan, Complete mineralization of the antibiotic amoxicillin by electro-Fenton with a BDD anode, J. Appl. Electrochem. 44 (2014) 1327-1335.

[35] H. Lin, J. Wu, N. Oturan, H. Zhang, M.A. Oturan, Degradation of artificial sweetener saccharin in aqueous medium by electrochemically generated hydroxyl radicals, Environ. Sci. Pollut. R. 23 (2016) 4442-4453.

[36] T.S. Chen, R.W. Tsai, Y.S. Chen, K.L. Huang, Electrochemical degradation of tetracycline on BDD in aqueous solutions, Int. J. Electrochem. Sc. 9 (2014) e8434.

[37] E. Brillas, I. Sirés, M.A. Oturan, Electro-Fenton process and related electrochemical technologies based on Fenton's reaction chemistry, Chem. Rev. 109 (2009) 6570-6631.

[38] X. Zhu, M. Tong, S. Shi, H. Zhao, J. Ni, Essential explanation of the strong mineralization performance of boron-doped diamond electrodes, Environ. Sci. Technol. 42 (2008) 4914-4920.

[39] C. Tai, J.F. Peng, J.F. Liu, G.B. Jiang, H. Zou, Determination of hydroxyl radicals in advanced oxidation processes with dimethyl sulfoxide trapping and liquid chromatography, Anal. Chim. Acta 527 (2004) 73-80.

[40] Q. Wang, S. Tian, J. Long, P. Ning, Use of Fe (II) Fe (III)-LDHs prepared by co-precipitation method in a heterogeneous-Fenton process for degradation of Methylene Blue, Catal. Today 224 (2014) 41-48.

[41] A. Dirany, I. Sirés, N. Oturan, A. Özcan, M.A. Oturan, Electrochemical treatment of the antibiotic sulfachloropyridazine: kinetics, reaction pathways, and toxicity evolution, Environ. Sci. Technol. 46 (2012) 4074-4082.

[42] A. Dirany, S.E. Aaron, N. Oturan, I. Sirés, M.A. Oturan, J.-J. Aaron, Study of the toxicity of sulfamethoxazole and its degradation products in water by a bioluminescence method during application of the electro-Fenton treatment, Anal. Bioanal. Chem. 400 (2011) 353-360.

[43] W.L. Yang, M.H. Zhou, N. Oturan, Y.W. Li, P. Su, M.A. Oturan, Enhanced activation of hydrogen peroxide using nitrogen doped graphene for effective removal of herbicide 2, 4-D from water by iron-free electrochemical advanced oxidation, Electrochim. Acta 297 (2019) 582-592.

[44] H. Lin, N. Oturan, J. Wu, V.K. Sharma, H. Zhang, M.A. Oturan, Removal of artificial sweetener aspartame from aqueous media by electrochemical advanced oxidation processes, Chemosphere 167 (2017) 220-227.

[45] Y. Wang, G. Zhao, S. Chai, H. Zhao, Y. Wang, Three-dimensional homogeneous ferrite-carbon aerogel: one pot fabrication and enhanced electro-Fenton reactivity, ACS Appl. Mater. Inter. 5 (2013) 842-852.

[46] R. Jinisha, R. Gandhimathi, S. Ramesh, P. Nidheesh, S. Velmathi, Removal of rhodamine B dye from aqueous solution by electro-Fenton process using iron-doped mesoporous silica as a heterogeneous catalyst, Chemosphere 200 (2018) 446-454.

[47] X. Long, Z. Wang, S. Xiao, Y. An, S. Yang, Transition metal based layered double hydroxides tailored for energy conversion and storage, Mater. Today 19 (2016) 213-226.

[48] M.A. Oturan, M. Pimentel, N. Oturan, I. Sirés, Reaction sequence for the mineralization of the short-chain carboxylic acids usually formed upon cleavage of aromatics during electrochemical Fenton treatment, Electrochim. Acta 54 (2008) 173-182.

[49] S. Garcia-Segura, E. Brillas, Mineralization of the recalcitrant oxalic and oxamic acids by electrochemical advanced oxidation processes using a boron-doped diamond anode, Water Res. 45 (2011) 2975-2984.

[50] P.A. Diaw, N. Oturan, M.D.G. Seye, A. Coly, A. Tine, J.J. Aaron, M.A. Oturan, Oxidative degradation and mineralization of the phenylurea herbicide fluometuron in aqueous media by the electro-Fenton process, Sep. Purif. Technol. 186 (2017) 197-206.

[51] A. Couto, L. Santos, J. Matsushima, M. Baldan, N. Ferreira, Hydrogen and oxygen plasma enhancement in the Cu electrodeposition and consolidation processes on BDD electrode applied to nitrate reduction, Appl. Surf. Sci. 257 (2011) 10141-10146.

[52] M.I. Vasquez, M. Garcia-Käufer, E. Hapeshi, J. Menz, K. Kostarelos, D. Fatta-Kassinos, K. Kümmerer, Chronic ecotoxic effects to Pseudomonas putida and Vibrio fischeri, and cytostatic and genotoxic effects to the hepatoma cell line

(HepG2) of ofloxacin photo (cata) lytically treated solutions, Sci. Total Environ. 450 (2013) 356-365.

[53] L. Liu, R. Li, Y. Liu, J. Zhang, Simultaneous degradation of ofloxacin and recovery of Cu (II) by photoelectrocatalysis with highly ordered TiO_2 nanotubes, J. Hazard. Mater. 308 (2016) 264-275.

[54] M.I. Vasquez, E. Hapeshi, D. Fatta-Kassinos, K. Kümmerer, Biodegradation potential of ofloxacin and its resulting transformation products during photolytic and photocatalytic treatment, Environ. Sci. Pollut. R. 20 (2013) 1302-1309.

Table captions

Table 1: The contents of different elements in raw CF and $Fe^{II}Fe^{III}$ LDH-CF cathodes.

Cathode	C1 s (%)	O1 s (%)	N1 s (%)	Fe2p (%)
Raw CF	75.11	23.71	0.27	0.91
Fe^{II} Fe^{III} LDH-CF	39.92	23.91	1.82	34.35

Table 2: Values of the apparent rate constant, k_{app} (min^{-1}) for decay kinetics of OFC with raw CF and $Fe^{II}Fe^{III}$ LDH-CF cathode.

Cathode	3.12 mA cm^{-2}	6.25 mA cm^{-2}	9.37 mA cm^{-2}	12.5 mA cm^{-2}
CF (0.1 mM Fe^{2+})	0.01	0.04	0.05	0.09
Fe^{II} Fe^{III} LDH-CF	0.03	0.11	0.18	0.19

Table 3: Intermediate products identified using HPLC and GC-MS analyses during the mineralization of OFC in heterogeneous EF with $Fe^{II}Fe^{III}$ LDH-CF cathode: J: 6.25 mA cm^{-2}, pH: 7, V: 230 mL, [Na_2SO_4]: 50 mM

Compound	Molecular mass (g mol^{-1})	Molecular structure	Retention time (min)	Analytical technique
OTP 2	261	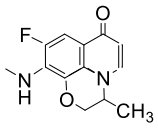	20.7	GC-MS
OTP 3	360	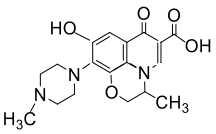	21.7	GC-MS
OTP 4	326	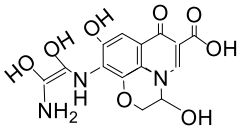	25.1	GC-MS
OTP 5	60	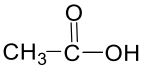	9.3	HPLC
OTP 6	116	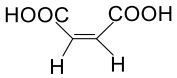	10.4	HPLC
OTP 7	90	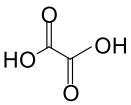	15.8	HPLC
OTP 8	116	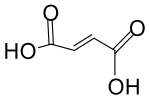	14.5	HPLC
OTP 9	89	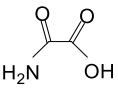	15.6	HPLC

Figure captions

Figure 1 SEM images of $Fe^{II}Fe^{III}$ LDH-CF cathode with different resolutions (a-c) and SEM-EDS-mapping of $Fe^{II}Fe^{III}$ LDH-CF (d-f).

Figure 2 SEM image and EDS analysis of $Fe^{II}Fe^{III}$ LDH-CF cathode without Fe particles (a) and with depositing Fe (b), XRD detection of $Fe^{II}Fe^{III}$ LDH-CF (c), XPS characterization of raw CF and $Fe^{II}Fe^{III}$ LDH-CF cathodes (d).

Figure 3 Linear sweep voltammetry (LSV) of the raw CF and $Fe^{II}Fe^{III}$ LDH-CF cathodes (a), Cyclic voltammetry (CV) detection of electrocatalytic activity towards Fe(III)/Fe(II) redox couple (b), Decay kinetics of OFC with raw CF (c) and $Fe^{II}Fe^{III}$ LDH-CF (d) electrodes: [OFC]: 0.1 mM, J: 6.25 mA cm^{-2}, pH: 7, V: 230 mL, [Na_2SO_4]: 50 mM, [Fe^{2+}]: 0.1 mM (only in EF system with raw CF)

Figure 4 Effect of current density on TOC removal and evolution of EC during OFC mineralization in heterogeneous EF with $Fe^{II}Fe^{III}$ LDH-CF cathode (a,b) and homogeneous EF with raw CF cathode (c,d) : [OFC]: 0.1 mM, J: 9.37 mA cm^{-2}, pH: 7, V: 230 mL, [Na_2SO_4]: 50 mM.

Figure 5 The evolution of pH (a), amounts of Fe^{2+} and total Fe leached (b) during the process of OFC mineralization in heterogeneous EF with $Fe^{II}Fe^{III}$ LDH-CF, comparative amounts of H_2O_2 generation and detected $^{\bullet}OH$ in homogeneous and heterogeneous EF(c), degradation efficiencies of OFC in heterogeneous EF, with addition of $^{\bullet}OH$ scavenger (tertiary butyl alcohol, TBA) and anodic oxidation with stainless steel (SS) cathode (d): [OFC]: 0.1 mM, J: 6.25 mA cm^{-2}, pH: 7, V: 230 mL, [Na_2SO_4]: 50 mM.

Figure 6 The stability and reusability of $Fe^{II}Fe^{III}$ LDH-CF electrode for the decay

kinetics of OFC (a) and TOC removal (b): [OFC]: 0.1 mM, J: 6.25 mA cm^{-2}, pH: 7, V: 230 mL, [Na_2SO_4]: 50 mM.

Figure 7 Evolution of carboxylic acids (a) and inorganic ions (b) during the process of OFC mineralization in heterogeneous EF with $Fe^{II}Fe^{III}$ LDH-CF: [OFC]: 0.1 mM, J: 9.37 mA cm^{-2}, pH: 7, V: 230 mL, [Na_2SO_4]: 50 mM.

Figure 8 Reaction pathway proposed for OFC degradation in heterogeneous EF.

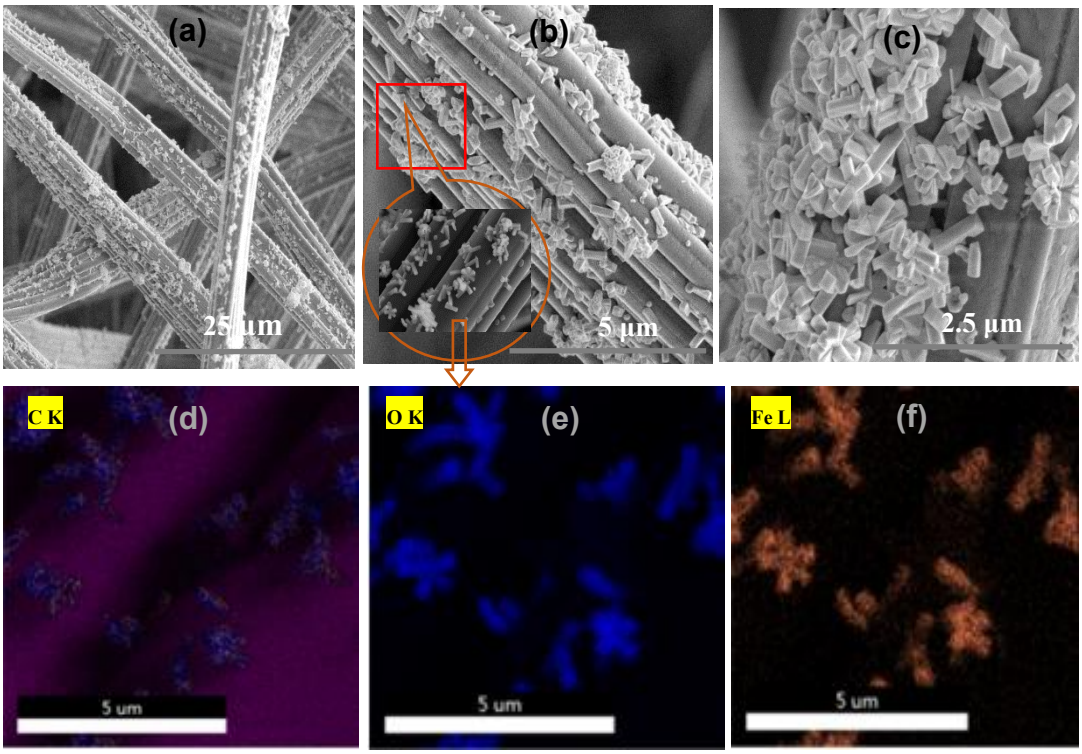

Fig. 1

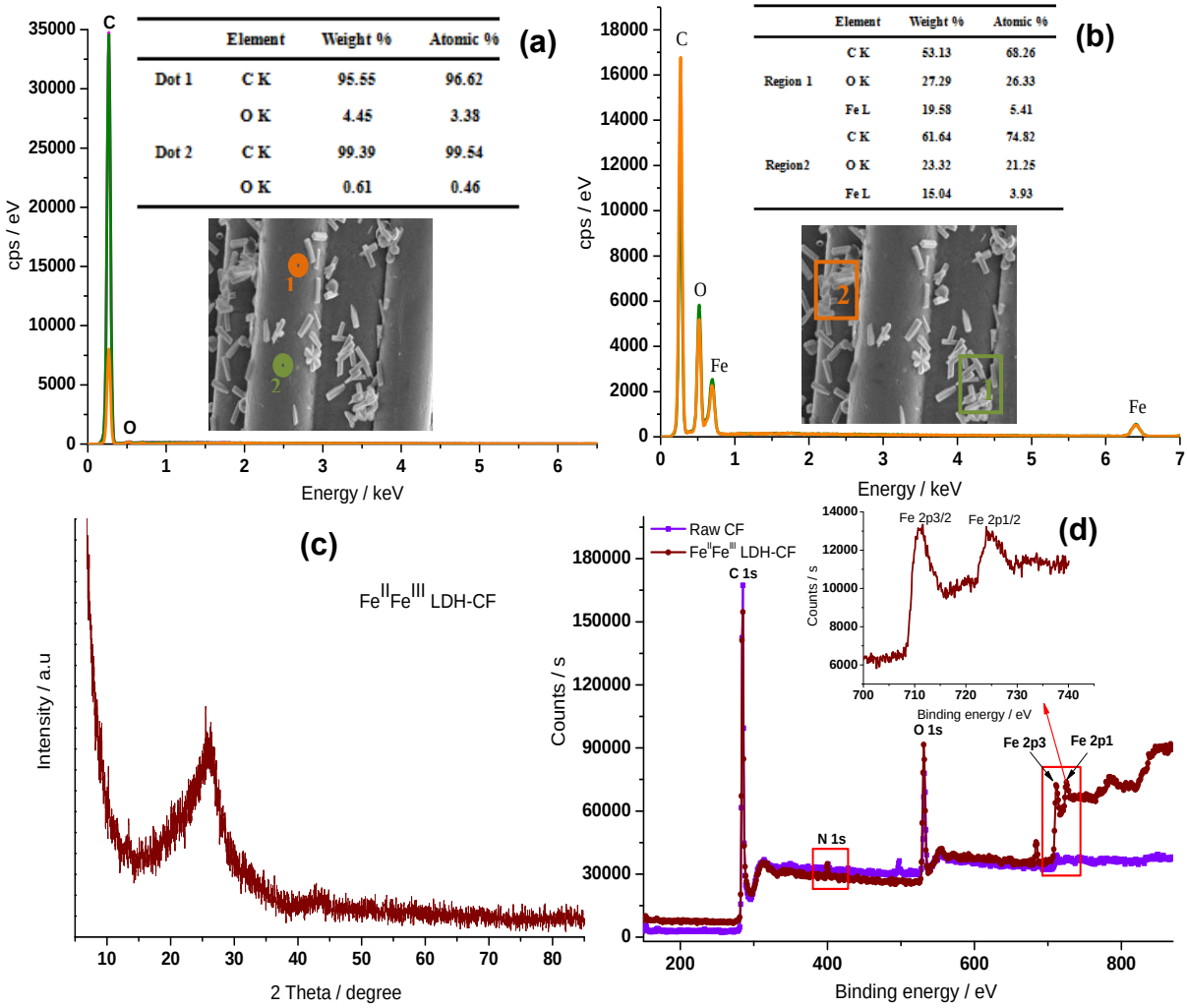
(a)
Element
Weight %
Atomic %
Dot 1
C K
95.55
96.62
O K
4.45
3.38
Dot 2
C K
99.39
99.54
O K
0.61
0.46
cps / eV
Energy / keV
C
O
(b)
Element
Weight %
Atomic %
Region 1
C K
53.13
68.26
O K
27.29
26.33
Fe L
19.58
5.41
Region2
C K
61.64
74.82
O K
23.32
21.25
Fe L
15.04
3.93
Fe
(c)
Fe^II Fe^III LDH-CF
Intensity / a.u
2 Theta / degree
(d)
Raw CF
Fe^II Fe^III LDH-CF
C 1s
O 1s
N 1s
Fe 2p3
Fe 2p1
Fe 2p3/2
Fe 2p1/2
Counts / s
Binding energy / eV

Fig. 2

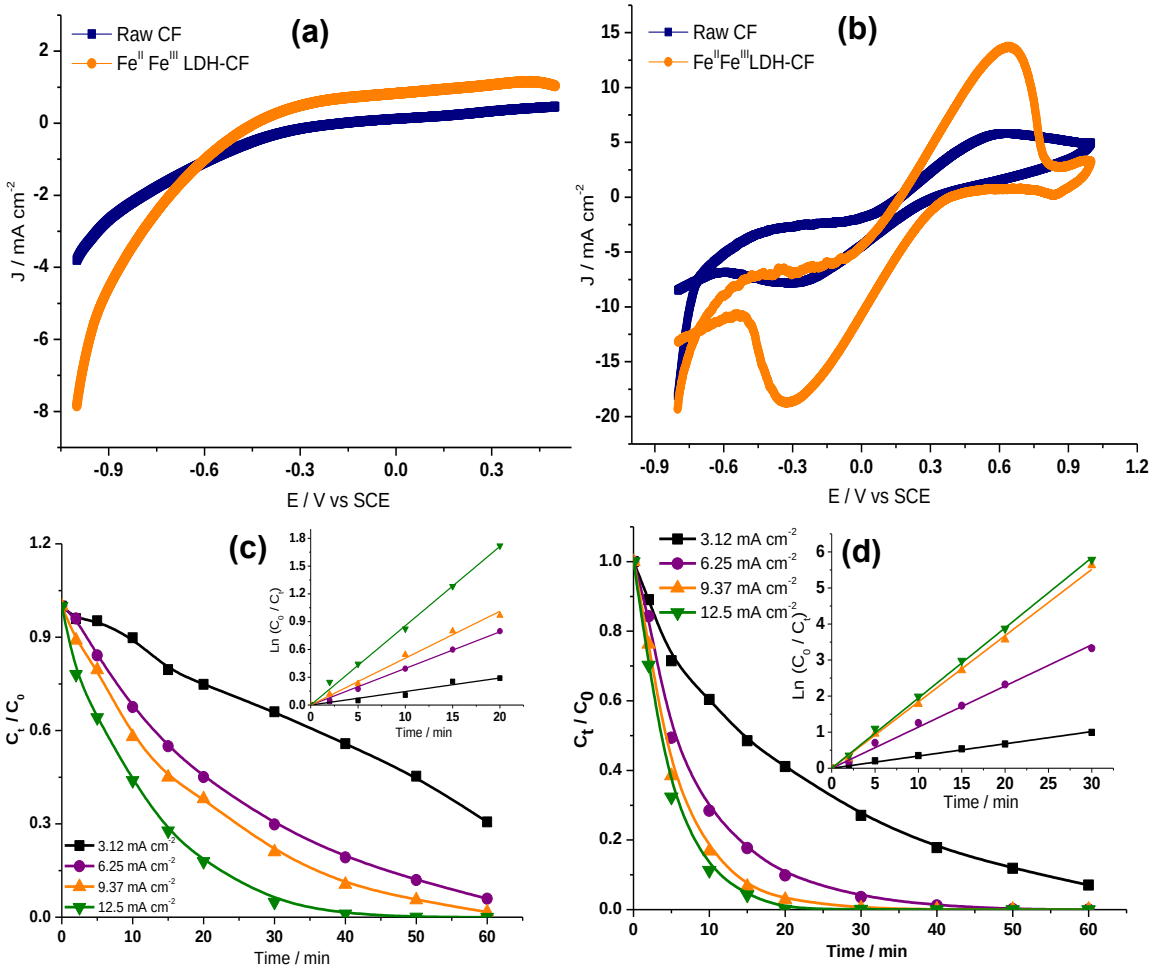
(a)
Raw CF
Fe^{II} Fe^{III} LDH-CF
J / mA cm^{-2}
E / V vs SCE
(b)
Raw CF
Fe^{II}Fe^{III}LDH-CF
J / mA cm^{-2}
E / V vs SCE
(c)
C$_t$ / C$_0$
Time / min
Ln (C$_0$ / C$_t$)
3.12 mA cm^{-2}
6.25 mA cm^{-2}
9.37 mA cm^{-2}
12.5 mA cm^{-2}
(d)
C$_t$ / C$_0$
Time / min
Ln (C$_0$ / C$_t$)
3.12 mA cm^{-2}
6.25 mA cm^{-2}
9.37 mA cm^{-2}
12.5 mA cm^{-2}

Fig. 3

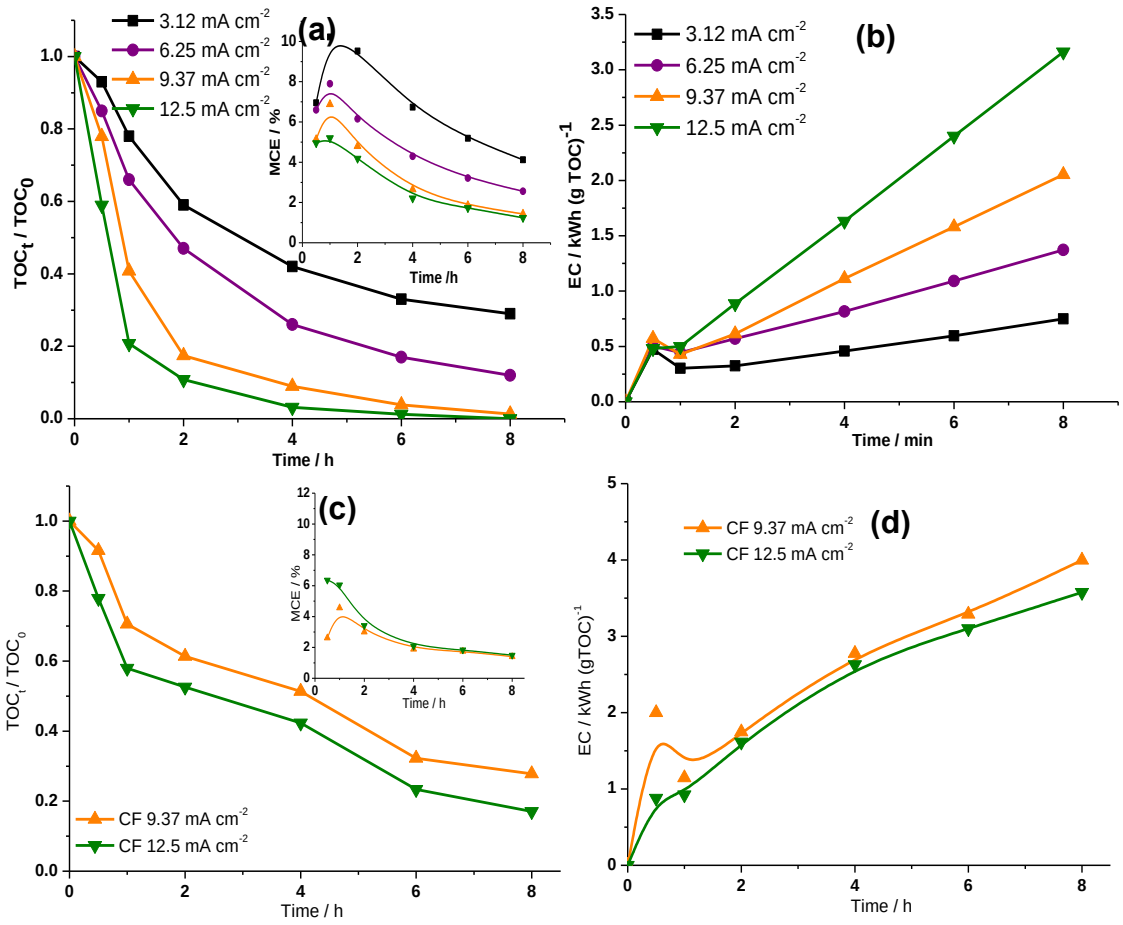

Fig. 4

Fig. 4 (d): The point for 0.5 h seems to be wrong. The deviation is very high (experimental error!). You can delete this point from the figure.

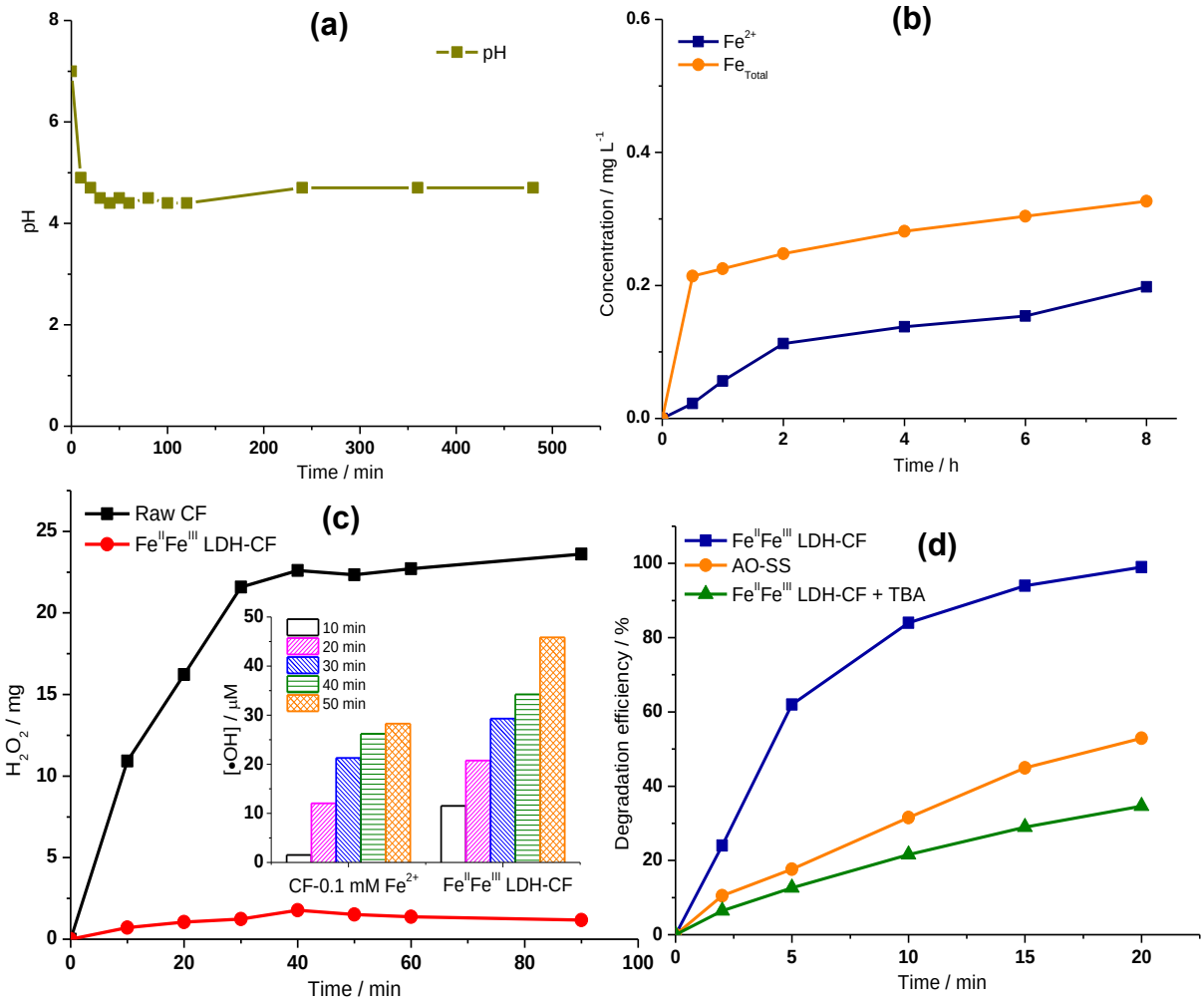

Fig. 5

Fig. 5 (c): unit ? mg per what volume ?, mg / L ?

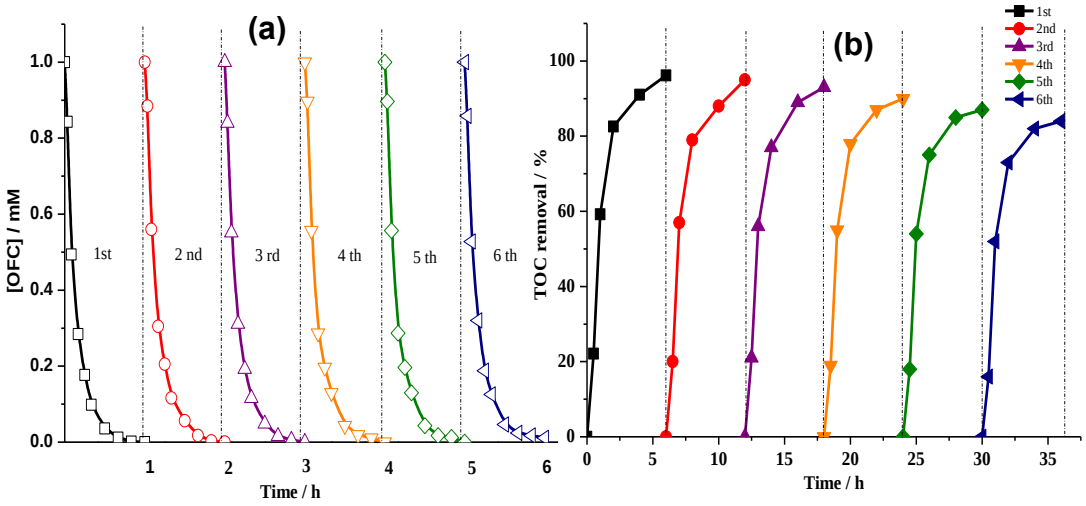
(a)
[OFC] / mM
1.0
0.8
0.6
0.4
0.2
0.0
1st
2 nd
3 rd
4 th
5 th
6 th
1
2
3
4
5
6
Time / h
(b)
TOC removal / %
100
80
60
40
20
0
0
5
10
15
20
25
30
35
Time / h
1st
2nd
3rd
4th
5th
6th

Fig. 6

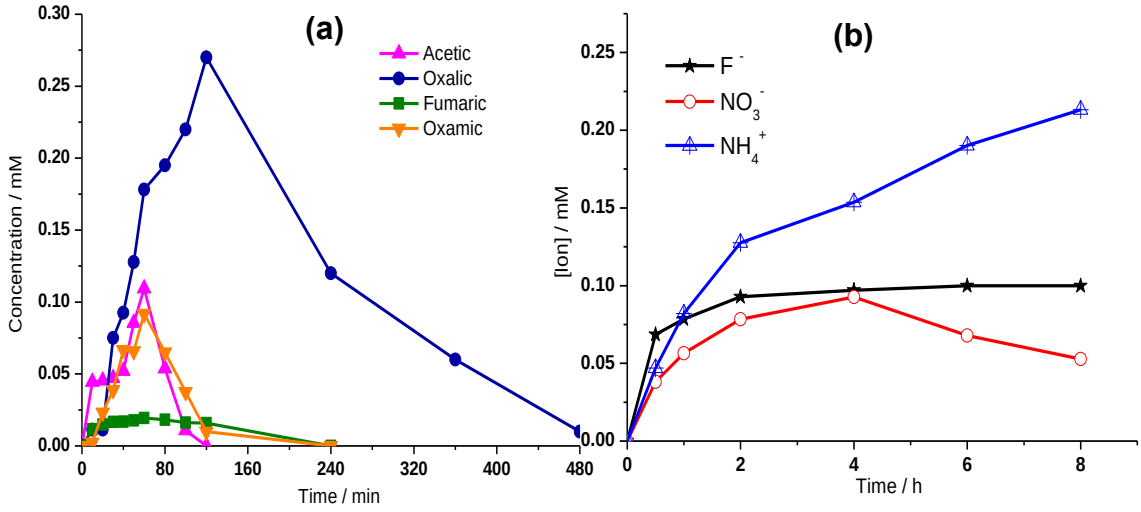
(a)
Acetic
Oxalic
Fumaric
Oxamic
Concentration / mM
Time / min
0.00
0.05
0.10
0.15
0.20
0.25
0.30
0
80
160
240
320
400
480
(b)
F -
NO3 -
NH4 +
[Ion] / mM
Time / h
0.00
0.05
0.10
0.15
0.20
0.25
0
2
4
6
8

Fig. 7

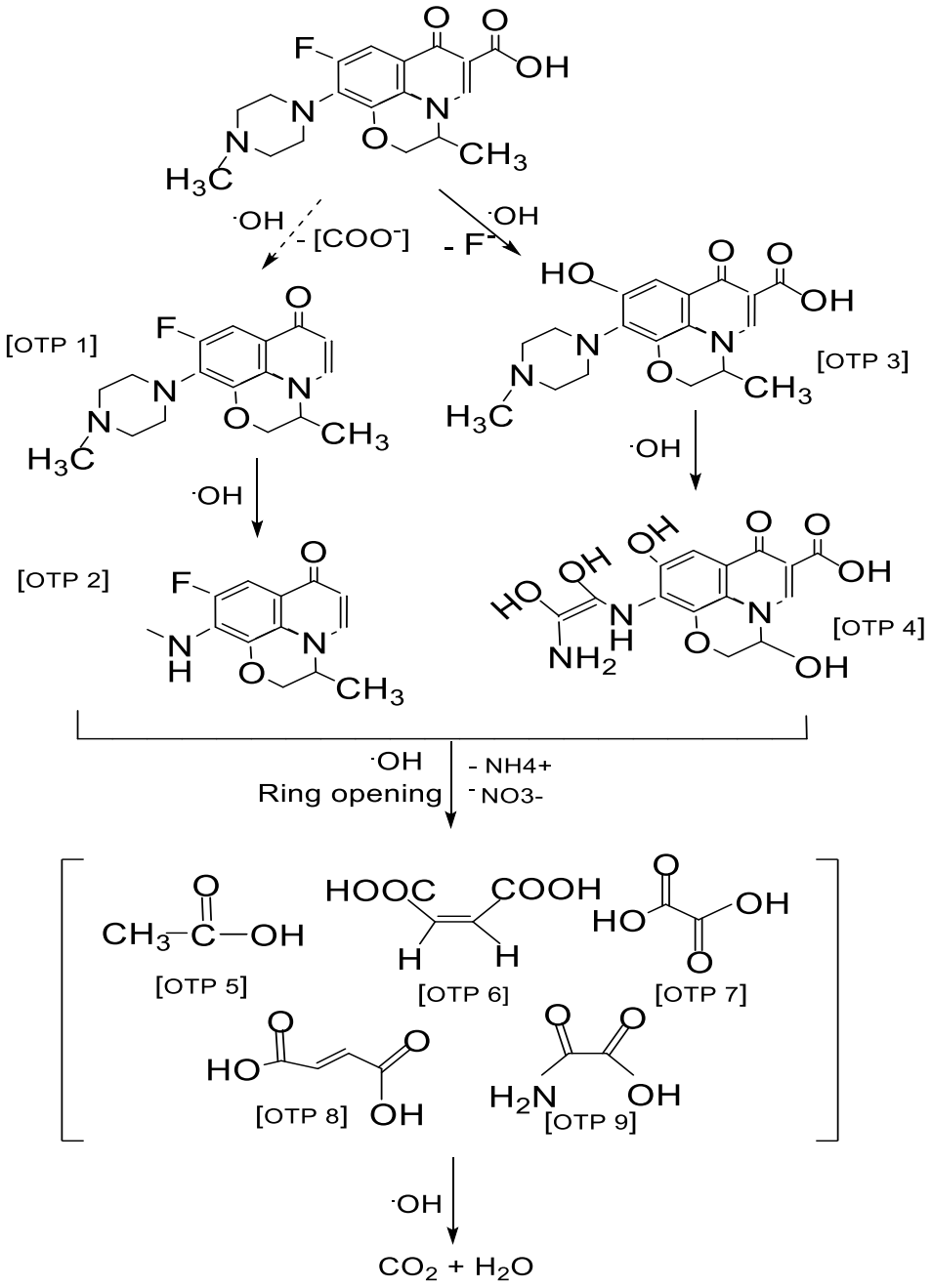
·OH
- [COO⁻]
·OH
- F⁻
[OTP 1]
[OTP 3]
·OH
·OH
[OTP 2]
[OTP 4]
·OH
Ring opening
- NH4+
- NO3-
[OTP 5]
[OTP 6]
[OTP 7]
[OTP 8]
[OTP 9]
·OH
CO2 + H2O

Fig. 8